Journal of Hazardous Materials 471 (2024) 134368

Contents lists available at ScienceDirect

Journal of Hazardous Materials

journal homepage: www.elsevier.com/locate/jhazmat

Research Paper

Role of municipal solid waste incineration fly ash components in co-pyrolysis of oily sludge: Pyrolysis products and catalytic mechanism

Di Yu [a,b,d], Zhiwei Li [a], Jie Li [a], Bo Li [d], Hao Yu [a], Jun He [b,e,*], Yin Wang [a,c,**]

[a] Key Laboratory of Urban Pollutant Conversion, Institute of Urban Environment, Chinese Academy of Sciences, Xiamen 361021, China
[b] Department of Chemical and Environmental Engineering, University of Nottingham Ningbo China, Ningbo 315100, China
[c] Zhejiang Key Laboratory of Urban Environmental Processes and Pollution Control, CAS Haixi Industrial Technology Innovation Center in Beilun, Ningbo 315830, China
[d] Department of Civil Engineering, University of Nottingham Ningbo China, Ningbo 315100, China
[e] Nottingham Ningbo China Beacons of Excellence Research and Innovation Institute, Ningbo 315100, China

HIGHLIGHTS

- The existence of $CaCO_3$ and $CaSO_4$ impedes the catalytic cracking of oil sludge.
- $CaCl_2$, KCl, and $Ca(OH)_2$ reduce coke yield and promote light aromatics formation.
- $Ca(OH)_2$ contributes the most to H_2 formation and increases it by 137.16 %.
- Alkali chlorides enhances the production of CO, CO_2, and gaseous hydrocarbons.
- IFA components promoted the reduction and dispersion of inherent Fe species in OS.

GRAPHICAL ABSTRACT

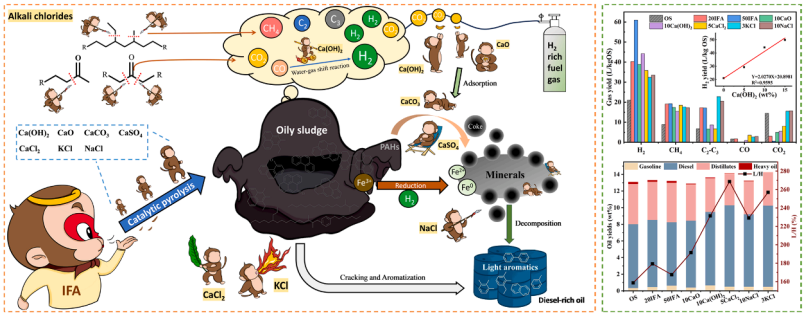

ARTICLE INFO

Keywords:
Co-pyrolysis mechanism
Incineration fly ash
Oily sludge
Oil upgrading
Hydrogen generation

ABSTRACT

The co-pyrolysis of oily sludge (OS) and municipal solid waste incineration fly ash (IFA) is a promising strategy for sustainable waste management. This study delves into the distinct catalytic roles of individual IFA components during co-pyrolysis and assesses their impact on the inherent Fe species in OS, highlighting their contributions to overall catalytic activity. Notably, in comparison to IFA, $CaCl_2$ and KCl significantly enhance pyrolysis oil upcycling, while IFA components collectively exhibit a positive catalytic effect on pyrolysis gas and coke production. $Ca(OH)_2$ notably boosts H_2 yield by 137.16 %. Alkali chlorides facilitate gaseous hydrocarbon formation and convert oxygen-containing compounds to CO and CO_2 which are subsequently consumed and absorbed by CaO and $Ca(OH)_2$. $CaCl_2$ and KCl promote heavy compound decomposition and alkane aromatization, reducing coke formation and increasing light aromatic production. Conversely, NaCl increases alkane proportions. However, $CaSO_4$ and $CaCO_3$ hinder catalytic reactions, promoting carbon conversion to coke. Importantly, IFA compounds aid the dispersion of inherent Fe-based species from OS on char surface, enhancing in-situ catalytic pyrolysis. Additionally, the augmented H_2 production accelerates the reduction of Fe-based species. The findings expand waste utilization possibilities and provide insights for co-processing solid wastes.

* Corresponding author at: Department of Chemical and Environmental Engineering, University of Nottingham Ningbo China, Ningbo 315100, China.
** Corresponding author at: Key Laboratory of Urban Pollutant Conversion, Institute of Urban Environment, Chinese Academy of Sciences, Xiamen 361021, China.
E-mail addresses: jun.he@nottingham.edu.cn (J. He), yinwang@iue.ac.cn (Y. Wang).

https://doi.org/10.1016/j.jhazmat.2024.134368
Received 21 February 2024; Received in revised form 8 April 2024; Accepted 18 April 2024
Available online 19 April 2024

1. Introduction

The petroleum industry continues to be an indispensable component of modern industrial operations; nevertheless, environmental concerns stemming from the harmless disposal of oily sludge (OS), widely recognized as a hazardous waste, has come to the forefront, demanding effective and sustainable solutions [1]. The abundant presence of toxic petroleum hydrocarbons in OS also underscores its potential as a valuable source of alternative fuel. In China, the annual production of OS ranges from 4.45 to 6.22 million tons, with an average rate of approximately 36 % for comprehensive utilization [2]. The cumulative historical stockpile exceeds 143 million tons, and this figure is continually growing [3]. Nonetheless, the presence of heavy metal ions, pathogens, and compounds containing nitrogen and sulfur in OS hinders its disposal and energy recovery [4], posing risks to both human health and ecological systems.

In recent years, pyrolysis has become an effective and environmentally friendly method for OS treatment due to its great advantages, including low secondary pollution, great volume reduction capacity, high energy recovery efficiency, and the ability to immobilize heavy metals [5–8]. Effective catalyst can accelerate the degradation of large molecular organic substances, increase pyrolysis gas and oil yields, and improve the quality of pyrolysis products. For example, zeolites with great pore structure could facilitate cracking reactions and improve the properties of pyrolysis products [9]. HZSM-5 zeolites incorporated with Zn could optimize the pyrolysis oil yield and increase the aromatics selectivity [10]. Multiple salts have been also applied as catalysts for OS pyrolysis, with KCl addition achieving the highest oil yield [11]. Zhang et al. [12] discovered that the intrinsic $CaCO_3$ present in petrochemical sludge exerted a neutralizing impact on the char functional groups and a reduction in thermal decomposition activation energy. Despite these benefits, the separation and recovery of these commercial catalysts from pyrolysis residues are challenging during in-situ catalysis. Additionally, coke deposition on the catalyst surface would cause deactivation of the catalyst, thereby, increasing the cost of catalytic pyrolysis. This highlights the demand for affordable alternative catalysts for OS pyrolysis.

Several waste-based substances have been utilized in OS catalytic pyrolysis. In a study by Gao et al. [13], the fly ash from sewage sludge gasification was used as the catalyst for OS pyrolysis, and a decrease of straight chain alkanes was observed. Lin et al. [14] investigated OS pyrolysis with the addition of red mud and steel slag, and the results showed a higher pyrolysis gas yield with increased H_2 selectivity. They also explored the catalytic effects of individual pristine oxides in red mud and found that Fe_2O_3 presented the best catalytic capacity.

Incineration fly ash (IFA) from municipal solid waste poses a disposal challenge. Due to its hazardous nature, IFA requires cement-based or chemical-based solidification/stabilization (S/S) before landfilling [15, 16]. Alternative technologies, such as cement clinker co-combustion [16,17], microwave-assisted hydrothermal method [18], and microwave sintering [19], primarily aimed to stabilize heavy metals and remove chlorides, overlooking the catalysis potential of IFA. In our previous study, the co-pyrolysis of OS and IFA initiated a series of intricate reactions that contributed to increased light oil formation, higher H_2 selectivity in pyrolysis gas, elimination of CO_2 emission, inhibited coke formation, and heavy metal stabilization [20].

Nevertheless, our previous study has only examined the effect of IFA as a catalyst on the distribution and properties of OS pyrolysis products [20]. There is still a lack of thorough exploration of the underlying catalytic mechanism due to the complicated compositions in IFA. Furthermore, reported studies mainly focused on catalytic roles of metal oxides [14], and neglected their inorganic forms present in waste materials such as chlorides, hydroxides, carbonates, and sulphates. These substances can potentially exhibit greater catalytic reactivity [21], which highlights the need for comprehensive investigations in waste material characterization. Heng et al., explored the catalytic impact of CaClOH in IFA on the pyrolysis of single-use plastics [22]. However, limited focus was placed on the other minerals present in IFA, and the individual contributions of each IFA component to the overall catalytic activity were not addressed. Moreover, previous studies consistently used a fixed catalyst addition ratio [14], overlooking the component proportions in waste materials, which can substantially influence catalytic outcomes [23]. Thus, these considerations guide our exploration of the catalytic mechanism of IFA on OS co-pyrolysis.

This study aims to expand on our previous research and investigate the role of each component in IFA to unravel the comprehensive catalytic mechanism of IFA on OS pyrolysis. We conducted catalytic pyrolysis of OS in a fixed bed reactor with individual pristine inorganic compounds in IFA, including Ca-bearing substances and chlorides, as additives. The properties of the pyrolysis oil, gas, and char were investigated thoroughly to draw conclusions about the catalytic impact and contributions of each IFA component. Meanwhile, XRD, XPS, and SEM-EDS were applied to pyrolysis chars to evaluate the potential synergies between IFA components and inherent Fe species in OS during the co-pyrolysis. These inquiries are not only vital for advancing the understanding of waste co-processing mechanisms but also offer practical implications for clean energy recovery, catalytic petroleum fuel processing, and environmental management.

2. Materials and methods

2.1. Materials

The tank bottom OS from a waste oil treatment plant in Ningbo, Zhejiang Province was used in this study. The IFA was obtained from bag filters in a stocker grate incineration plant operating by Everbright Environmental Energy (Ningbo) Co., Ltd. The feedstocks were heated in an oven at 105 °C for 12 h before use and characterization. The physiochemical properties of the OS and IFA were listed in Table 1, and the proportions of oil and solid fractions in the OS were determined according to ASTM D95–13 [24]. As depicted in Fig. S1, X-ray Diffraction (XRD) analysis using X'Pert Pro was conducted to identify the inorganic compositions of both IFA and OS solid fractions. The main inorganic compounds in IFA were determined combined with previous references [25–27], which contains CaO, $CaCO_3$, $Ca(OH)_2$, $CaCl_2$, $CaSO_4$, KCl, and NaCl. The selected chemicals in the analytical grade were purchased from Sinopharm Chemical Reagent Co., Ltd. as additives in this study. To maximize the observed effects, the chemicals were blended with OS at a

Table 1
Physicochemical properties of OS and IFA (Oxygen content was determined through O %=100-C %-H %-N %-ash %).

Samples	OS	IFA
Moisture(wt%)	17.31	2.59
Proximate analysis (wt%, dry basis)		
Ash	48.28	82.50
Volatile matter	38.89	17.26
Fixed carbon	12.83	0.24
Ultimate analysis (wt%, dry basis)		
C	38.28	2.80
H	4.52	1.78
O	8.54	12.49
N	0.38	0.43
S	9.24	2.79
Inorganic elements (oxide form, %)		
CaO	14.83	52.73
Cl	0.15	20.96
Na_2O	0.55	10.55
SO_3	22.27	7.47
K_2O	0.15	3.86
Fe_2O_3	24.41	0.45
SiO_2	12.52	1.62
MgO	0.63	0.69
ZnO	0.35	0.57
Al_2O_3	11.80	0.38

specific ratio based on the proximate proportions of Ca, Cl, Na, S, K, and Fe in 50 wt% IFA as determined by X-ray fluorescence (Axios-MAX) results (Table 1). In detail, KCl was added at a ratio of 3 wt%, $CaCl_2$ at 5 wt%, and NaCl at 10 wt%. Additionally, thermogravimetric (TG) analysis (Fig. S2) was performed on IFA by a TG analyzer (Netzsch TG 209 F3) to calculate the $Ca(OH)_2$ and $CaCO_3$ content in IFA [20], which are 34.17 wt% and 19.08 wt% respectively. To facilitate a better comparison of the catalytic effects of different calcium-bearing substances in IFA, the addition ratios of CaO, $CaCO_3$, and $CaSO_4$ were set at 10 wt%. Given that $Ca(OH)_2$ accounts for the highest proportion in IFA, addition ratios of 5 wt% and 15 wt% were investigated additionally. The additives and OS were blended in specified ratios and stirred for 15 min to achieve homogeneity. For convenience, the mixed sample blends were labelled as 10CaO, 5$Ca(OH)_2$, 10$Ca(OH)_2$, 15$Ca(OH)_2$, 5$CaCl_2$, 10NaCl, 3KCl, 10$CaCO_3$, and 10$CaSO_4$, respectively.

2.2. Pyrolysis apparatus

Fig. S3 presents the schematic diagram of this study. Thermogravimetric and derivative thermogravimetric (TG-DTG) analyses were performed using a thermogravimetric analyzer (Netzsch TG 209 F3, Germany), and a thermogravimetry baseline was established before experiment. The sample, weighing between 40–50 mg, was placed into the TG reactor, and subjected to heating at a rate of 10 °C min^{-1} from 40 °C to 800 °C. To eliminate non-condensable gas products, a flow rate of 60 mL min^{-1} N_2 was maintained throughout the process.

A fixed bed reactor system was applied for pyrolysis (Fig. S4), as reported in our previous work [20]. It comprises of gas feeding system, pyrolysis system, liquid and gas collecting system. For each experiment, about 50 g feedstock was loaded in the middle of vertical tubular furnace. N_2 controlled at 150 mL min^{-1} was supplied as carrier gas to transmit the gaseous phase. The final temperature was set as 600 °C [20] with a heating rate of 10 °C min^{-1}, and then held for 60 min. The volatiles produced in the reactor passed through a condenser and were retained in oil condenser and oil scrubbers. The incondensable gases were collected in gas bag, and the total gas volume was recorded by the wet gas meter. The solid residue remaining in the tube was collected as pyrolysis char. Acetone was utilized to cleanse the condenser, oil container, and oil scrubbers, ensuring the comprehensive collection of pyrolysis oil. To remove water and obtain the pyrolysis oil, excess $MgSO_4$ was introduced into the collected liquid mixture. Subsequently, rotary evaporation in a rotary vacuum evaporator at 27 °C was employed to separate the pyrolysis oil from the acetone solution. The extracted oil was then weighed and analyzed to determine its yield and composition. These experiments were conducted at least three times to ensure reproducibility.

2.3. Analytical methods

Oil and char yields were acquired based on weighting, and the mass of the gas component was calculated by subtraction. The oil yield $Y_{oil(daf)}$ (wt%), char yield $Y_{char(daf)}$ (wt%), and gas yield $Y_{g(daf)}$ (wt%) were calculated by the Eqs. (1) to (3) to evaluate the distributions of the pyrolysis products. Crucially, the char yield of OS was obtained after subtracting the mass of additives.

$$Y_{oil(daf)} = \frac{M_{oil}}{M_{OS}} \times 100\% \tag{1}$$

$$Y_{char(daf)} = \frac{M_{solid} - M_{additive} \times (1 - mass \quad loss\%)}{M_{OS}} \times 100\% \tag{2}$$

$$Y_{gas(daf)} = 100wt\% - Y_{oil(daf)} - Y_{char(daf)} \tag{3}$$

where M_{OS}, $M_{additive}$, M_{oil}, and M_{solid} denote the masses of OS, additives, pyrolysis oil and solid residue (kg), respectively. *mass loss*% of $Ca(OH)_2$ was 21.60 % (Fig. S2) and 0 for other chemicals due to their considerable thermal stability within 600 °C.

Micro-GC (Agilent 3000A) containing FID (capillary column) and TCD (5A molecular sieve and PQ) was applied to the pyrolysis gas to obtain the volume yield of each gas component, denoted as $Y_{gV(daf)}$, as determined by Eq. (4). FID mainly analyzed organic gas (C_2H_6, C_2H_4, C_3H_8, C_3H_6 (C2–C3), and CH_4), and TCD mainly analyzed inorganic gas (CO, CO_2, and H_2).

$$Y_{gV(daf)} = \frac{V_{gas(daf)} \times V_j\%}{m_{OS}} \tag{4}$$

where $V_{gas(daf)}$ represents the pyrolysis gas volume (L), and V_j% refers to the volumetric percentage of each gas component from GC result.

The boiling point distribution of the pyrolysis oil was obtained using simulated distillation gas chromatography (SCION 456-GC) following the ASTM D2887 [20]. Based on their boiling point distribution, the pyrolysis oil is classified into four different commercial oil products by this method: Gasoline (<180 °C), Diesel (180 °C~350 °C), Distillates (350 °C~500 °C), and Heavy oil (>500 °C) [28]. The yield of each oil fraction $Y_{i(daf)}$ (wt%) was calculated as Eq. (5).

$$Y_{i(daf)} = Y_{oil(daf)} \times m_i\% \tag{5}$$

where m_i% represents the weight ratio of each fraction in the total oil.

The pyrolysis oil compositions were analyzed using GC/MS (Agilent 7890 A/5975 C) with reference to the standard spectra in the NIST 05 standard mass spectrometry library.

Prior to characterization, the pyrolysis chars were pulverized into a fine powder and sieved through a 75 μm sieve. Following this, they were subjected to drying at 105 °C for 12 h. The quantification of carbon coke yield was achieved by hydrochloric acid washing as our previously reported [20]. An elemental analyzer (Vario MAX) was applied to measure the total carbon content in chars $C_{TC(daf)}$ (mg/g char) and the carbon content in residue after washing $C_{TOC(daf)}$ (mg/g residue). Afterwards, the carbon coke content $C_{coke(daf)}$ and the carbon coke yield $Y_{coke(daf)}$ (wt %) can be calculated by Eqs. (6) and (7), respectively.

$$C_{coke(daf)} = \frac{C_{TOC(daf)} \times m_{washed \quad residue}}{m_{solid}} \tag{6}$$

$$Y_{coke(daf)} = C_{coke(daf)} * \frac{m_{solid}}{m_{OS}} \times 100\% \tag{7}$$

where $m_{washed\ residue}$ represents the mass of residue after HCl washing.

The mineral composition of the pyrolysis chars was analyzed using X-ray Diffraction (XRD) with Cu Kα radiation (40 kV, 40 mA), covering a scanning range of 10° to 90° (2θ) at a rate of 10°/min and performed at 20 °C. Phase identification utilized the ICDD PDF-2 2004 database. Fourier Transform Infrared Spectroscopy (FTIR) with a range of 400–4000 cm^{-1} was employed to investigate surface functional groups. For FTIR analysis, samples were prepared using the tablet compression method, grinding 1–2 mg samples with approximately 100 mg dry potassium bromide (a.r.) powder into a fine powder mixture, then pressing into pellets. X-ray Photoelectron Spectroscopy (XPS) with an Al Kα X-ray source (Axis Supra) was utilized to examine the valence state of iron. Lastly, Scanning Electron Microscopy (SEM) combined with Energy Dispersive X-ray Spectroscopy (EDX) (S-4800) was employed to study the microstructure of the pyrolysis chars and detect element distributions on char surfaces.

3. Results and discussion

To emphasize the role of individual components in the overall catalytic effect of IFA during OS co-pyrolysis, two additional groups of data (20IFA and 50IFA) obtained from co-pyrolysis of OS and IFA are included for comparison [20], since 50IFA is the basis for selecting the

addition ratio of these inorganic compounds and 20 wt% is the optimal addition ratio of IFA for the co-pyrolysis.

3.1. TG-DTG results of co-pyrolysis of oily sludge and incineration fly ash

The TG results from co-pyrolysis of OS and IFA at a mass ratio of 1:1 imply a positive catalytic effect of IFA on OS pyrolysis, as shown in Fig. 1 (b). Previous studies [13,14] neglected the mass loss of waste-based additives, but it is found that IFA is not entirely thermal stable (Fig. S2). Thereby, the weight loss of IFA during co-pyrolysis was considered, and the TG results of OS and IFA are presented in Fig. 1(a). The theoretical mass loss of 50IFA $Mass\%_{50IFA-theo}$, as calculated by Eq. (8) aims to determine the variation of mass loss when no interactions take place between IFA and OS during the co-pyrolysis, therefore, the differences between the experimental and theoretical results could identify the effects of possible interactions between IFA and OS.

$$Mass\%_{50IFA-theoretical} = 50\% \times Mass\%_{IFA} + 50\% \times Mass\%_{OS} \quad (8)$$

where $Mass\%_{IFA}$ and $Mass\%_{OS}$ are the experimental mass ratio of IFA and OS at each temperature in Fig. 1(a), respectively.

As shown in Fig. 1(b), the DTG curve of experimental results is above the theoretical results (170 °C-350 °C), demonstrating the addition of IFA enhances the heat transfer rate due to its improved physical transfer capacity. Furthermore, the increased mass loss rate of the experimental results between 650 °C and 750 °C can be attributed to the decomposition of carbonates [14]. It can be confirmed that these carbonates are formed from the adsorption of CO_2 released during the thermal decomposition of organic substances by calcium-bearing inorganic compounds in IFA [20]. This phenomenon can also explain the variation between 346 °C and 423 °C is attributed to the CO_2 adsorption, which result in reduced DTG peak observed in the experimental one. At 800 °C, most carbonates are decomposed, and the residual mass of experimental result is 61.97 % which is much lower than the theoretical one (67.81 %). This result demonstrates that more organic substances in OS were decomposed during the co-pyrolysis, suggesting that IFA benefited oily sludge pyrolysis.

3.2. Catalytic pyrolysis of OS with individual IFA compounds addition

3.2.1. Pyrolysis products distribution

The introduction of different inorganic compounds in IFA had distinguished impacts on the distributions of pyrolysis products, as shown in Fig. 2. Since the evaluation of carbon conversion by char yield is interfered by the absorbed CO_2, the yield of carbon coke, resulting from the condensation and polymerization of organic substances [29,30], becomes an essential index. The increased char yield and decreased gas yield observed in 10CaO and 10Ca(OH)$_2$ are consistent with our previous assumption that these compounds could achieve the CO_2 sequestration in pyrolysis char, which explains the same phenomenon observed in 20IFA and 50IFA. A slight decrease in carbon coke yield was also observed with 10 wt% CaO and 10 wt% Ca(OH)$_2$ addition. However, Li et al. [31] reported that CaO addition led to increased coke formation with high thermal stability. This discrepancy may be due to the omission of the accumulation of $CaCO_3$ in char. Conversely, the addition of 10 wt% $CaCO_3$ and $CaSO_4$ resulted in increased carbon coke yields as well as char yields, which might relate to enhanced condensation reaction [32]. Combined with the significantly decreased gas yield in 10$CaSO_4$ and oil yield in 10$CaCO_3$, it can be inferred that both $CaCO_3$ and $CaSO_4$ may inhibit the decomposition of heavy compounds in OS into volatile compounds and result in the formation of macromolecular intermediates [33].

Despite marginal variations in char yield, the additions of 10 wt% NaCl, 3 wt% KCl, and 5 wt% $CaCl_2$ effectively reduced the coke yield from 12.95 wt% to 11.22 wt%, 11.10 wt%, and 10.96 wt%, respectively, indicating their anti-coke property. Moreover, the addition of 3 wt% KCl and 5 wt% $CaCl_2$ led to increases in oil yield by 1.16 % and 1.04 %, respectively. Furthermore, the gas yield was also increased in 5$CaCl_2$ and 10NaCl. These findings suggested that alkali chlorides are highly active in promoting the decomposition of macromolecular compounds and facilitating the secondary cracking reaction, which align with the catalytic effects of alkali metals [34,35].

The theoretical pyrolysis product yields of 50IFA represent the average values obtained from the pyrolysis of OS with the addition of individual IFA components, as depicted in Fig. S5. By comparing these values to the experimental results of 50IFA, the impact of synergies among the major IFA components on the OS pyrolysis product distributions are identified. The higher char yield observed in experimental result is in line with the increased coke yield, suggesting that the presence of combinations of these additives in excess concentrations may diminishes the surface contact between the active sites of the catalyst and the active free radicals in chars [36], subsequently leading to the accumulation of these free radicals and enhancing polymerization [37,38]. Moreover, the relatively lower oil and gas yields of experimental results further support that the decomposition of heavy compounds and the secondary cracking were weakened due to the synergistic effects of multiple components.

As most inorganic compounds in IFA promoted the carbon conversion from solid into gas and oil products, their catalytic effects can explain the decreased carbon coke yield and increased oil yield in 20IFA and 50IFA. However, the addition of 10 wt% $CaCO_3$ and 10 wt% $CaSO_4$ promoted coke formation. Considering their negligible or negative effects on upgrading pyrolysis products during OS pyrolysis and their less active catalytic nature, the pyrolysis gas and oil compositions of

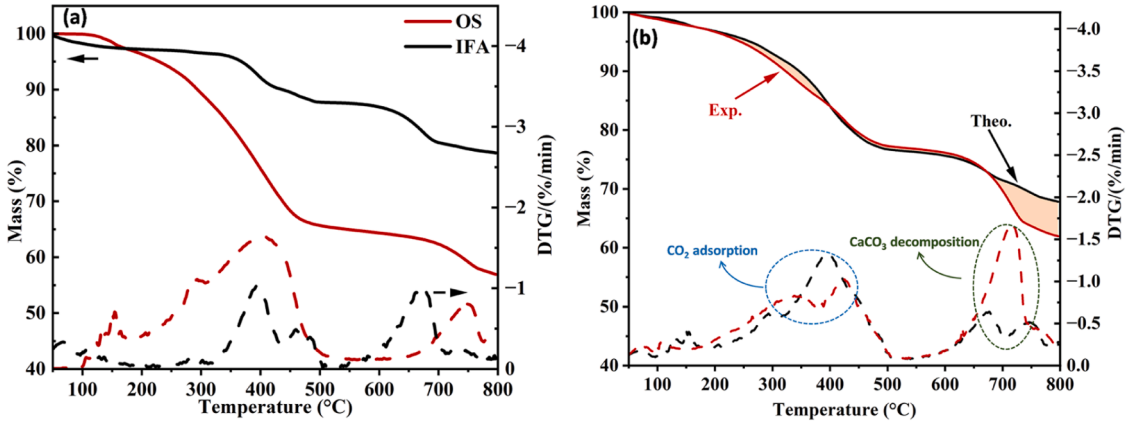

Fig. 1. TG-DTG curves of (a) individual pyrolysis of OS and IFA, (b) co-pyrolysis of OS and IFA at a mass ratio of 1:1 (theoretically calculated and experimentally measured).

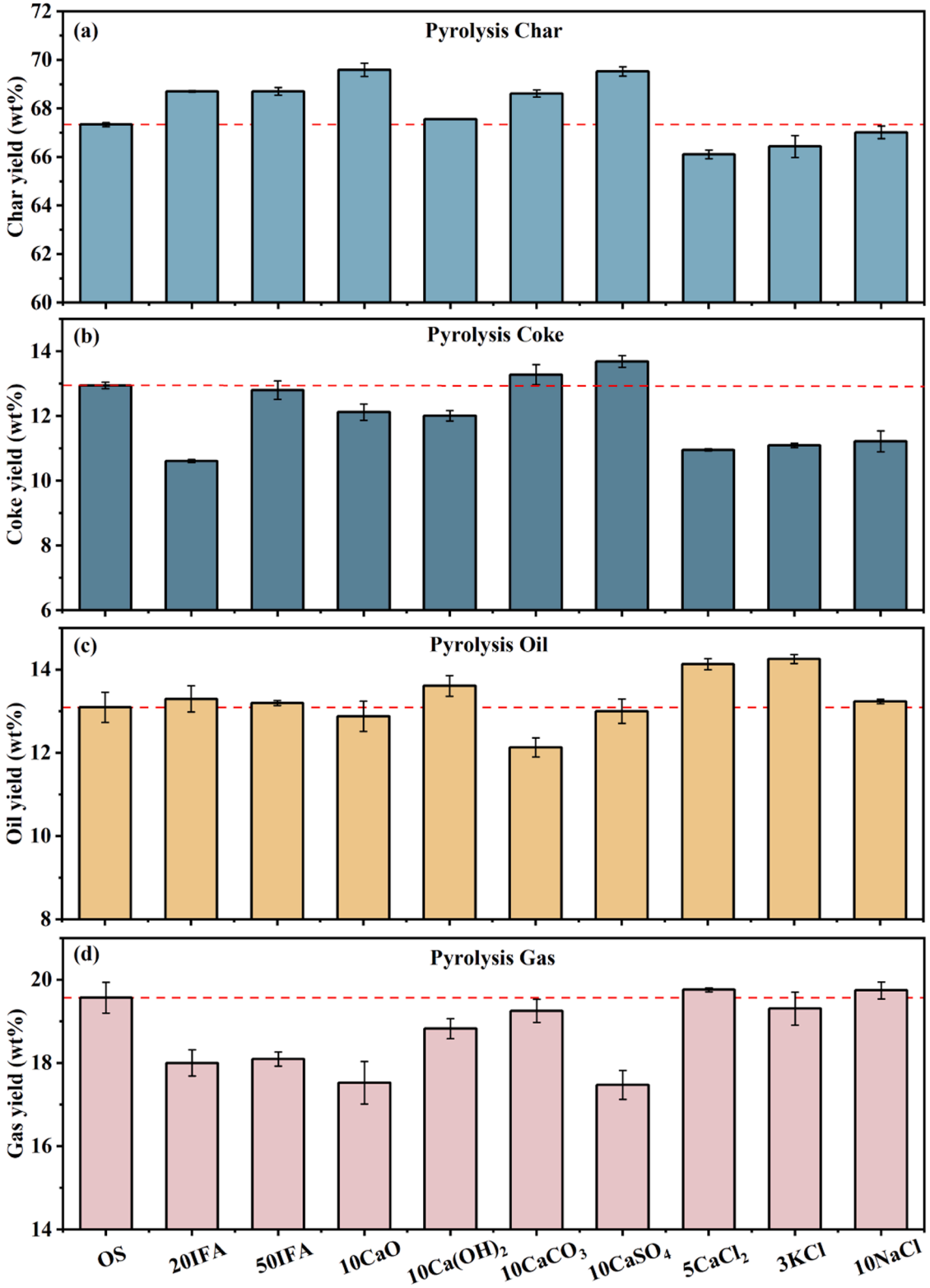

Fig. 2. Effects of inorganic compounds addition on (a) char yield, (b) coke yield, (c) oil yield, and (d) gas yield from oily sludge pyrolysis.

$10CaSO_4$ and $10CaCO_3$ were not further studied.

3.2.2. *Pyrolysis gas characterization*

The composition of OS pyrolysis gas underwent significant change with the addition of various inorganic compounds, as illustrated in Fig. 3 (a). With the addition of each inorganic compound, the dehydrogenation reaction and water-gas shift reaction were promoted [39], leading to significant increase in the H_2 yield. Among them, Ca-bearing substances showed a stronger effect than chlorides, and $10Ca(OH)_2$ resulted in the highest H_2 yield (44.20 L/kgOS), as shown in Fig. 3(b). Notably, negligible CO_2 was detected in $10Ca(OH)_2$ and 10CaO (5.45 and 4.95 L/kgOS, respectively), further proving their strong CO_2 adsorption capacity. On the other hand, the addition of NaCl, KCl, and $CaCl_2$ increased CO and CO_2 yield, implying alkali and alkaline earth metals

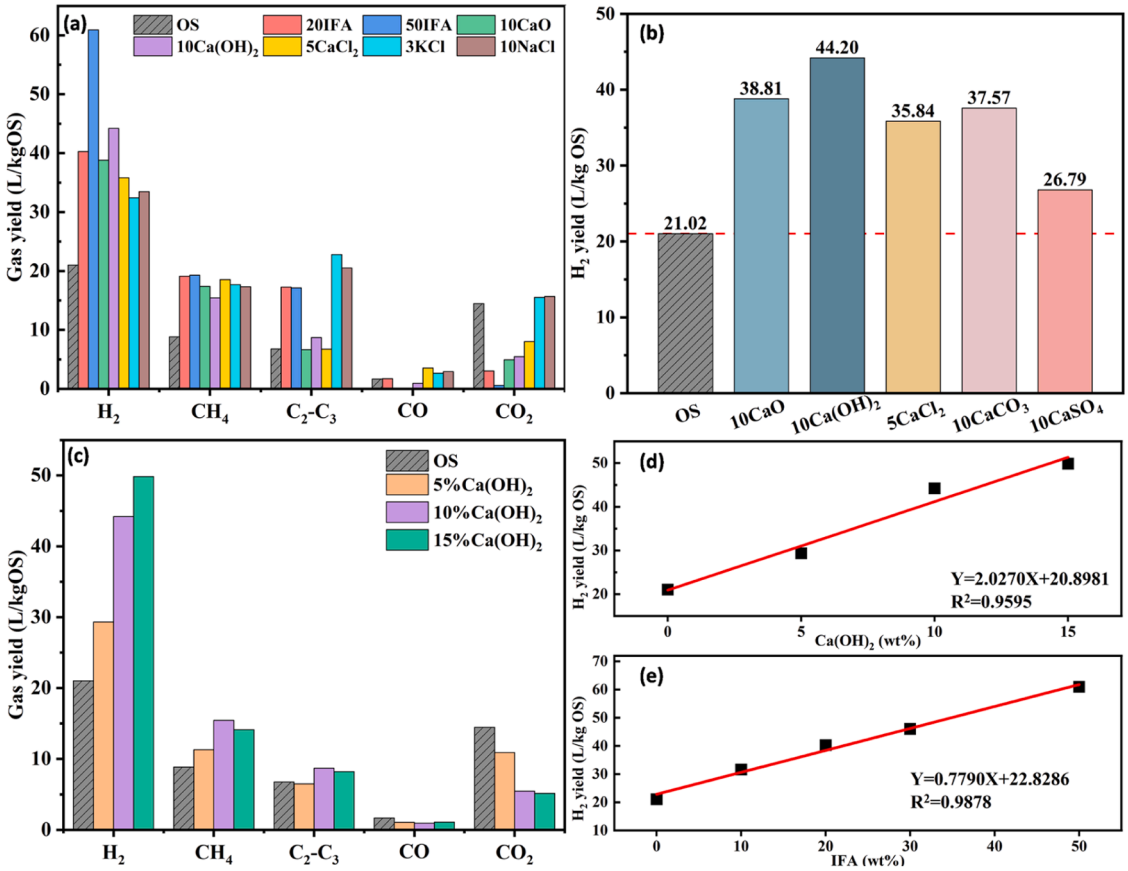

Fig. 3. Effects of (a) IFA components addition on pyrolysis gas composition, (b) different Ca-bearing inorganic compounds addition on H_2 yield, (c) $Ca(OH)_2$ addition ratios on pyrolysis gas compositions, and the linear relationship between (d) $Ca(OH)_2$ addition ratios with H_2 yield and (e) IFA addition ratios with H_2 yield.

could assist the deoxygenation reactions [35,40,41]. All IFA components promoted the formation of CH_4. Notably, compared to $5CaCl_2$ and other Ca-bearing compounds, 3KCl and 10NaCl significantly increased the yields of C2 and C3 hydrocarbons, indicating that alkali metal chlorides have a relatively stronger activation effect on the cracking reactions of macromolecule volatiles [42,43] and can promote gas products generation [44,45].

Considering $Ca(OH)_2$ as the primary component of IFA, an analysis of pyrolysis gas composition was conducted with varying $Ca(OH)_2$ addition ratios, as shown in Fig. 3(c). Notably, a substantial linear increase in H_2 yield was observed as $Ca(OH)_2$ addition ratios ranged from 0 to 15 wt%, as illustrated in Fig. 3(d). This finding is consistent with our previous observation of a linear relationship between IFA addition ratios with H_2 yield (Fig. 3e) [20]. It implies the possibility that $Ca(OH)_2$ played the predominant role in enhancing H_2 formation and could exhibit a continuous promoting effect within the tested range of addition ratios (10–50 wt% IFA). Gaseous hydrocarbon production reached peak in $10Ca(OH)_2$, and further increasing the addition ratio showed no significant impact on the generation of these gases. The limited CO detected indicates that it may react with H_2O released from the decomposition of $Ca(OH)_2$ and polymerization reactions through the water-gas shift reaction (Eq. 9). This reaction enhanced H_2 production, assisting the explanation of the higher H_2 yield in $10Ca(OH)_2$ compared to 10CaO. Furthermore, the adsorption capacity of $Ca(OH)_2$ for CO_2 was enhanced at higher addition ratios, which further shifted the water-gas shift reaction to the right-hand side and also explains the decreased yields of CO and CO_2 in 20IFA and 50IFA.

$$CO + H_2O \leftrightarrow CO_2 + H_2 \quad (9)$$

3.2.3. *Pyrolysis oil characterization*

Fig. 4 illustrates the effect of inorganic compounds addition on the quality and composition of OS pyrolysis oil. The addition of each inorganic compound led to an increase in the gasoline and diesel yields (Fig. 4b). The addition of 10 wt% $Ca(OH)_2$ achieved the highest gasoline yield of 0.68 wt%, which indicates its dominant role in promoting gasoline production in 50IFA. The increase in the yield of diesel, the primary component in pyrolysis oil, was most pronounced with 5 % $CaCl_2$ addition, which increased from 7.67 wt% to 9.78 wt%, followed by 3KCl (9.76 wt%). Furthermore, the incorporation of $CaCl_2$ decreased distillate production by 0.99 wt%, consisting with its notable catalytic effect observed in the pyrolysis of bitumen within shale matrices [46]. Here, we define gasoline and diesel as light oil fraction, while distillates and heavy oil are referred to as heavy oil fraction. Significantly, the addition of each catalyst led to the elimination of heavy oil, resulting in a notable improvement in the ratio of the light oil fraction to the heavy oil fraction (L/H). Among them, $5CaCl_2$ achieved the highest L/H of 268.68 % which increased by 109.98 % against non-catalytic pyrolysis of OS (158.69 %). However, the addition of 10 wt% CaO had a less significant effect on pyrolysis oil upcycling.

To conduct a comprehensive analysis of the pyrolysis oil compositions, the results obtained from GC-MS (Fig. S6) are presented in Fig. 4 (a). Similar to IFA, most selected inorganic compounds reduced the proportion of alkenes and promoted the formation of aromatics. Notably, as shown in Fig. 4(c), the addition of 3 wt% KCl, 10 wt% $Ca(OH)_2$, and 5 wt% $CaCl_2$ resulted in the most significant variations, increasing the aromatic proportion by 5.66 %, 5.48 %, and 5.04 %, respectively. This suggests these compounds not only promote the formation of lighter hydrocarbons but also significantly enhance the production of aromatics, which arise from reactions including dehydrogenation, deoxygenation, cyclization, and polycondensation

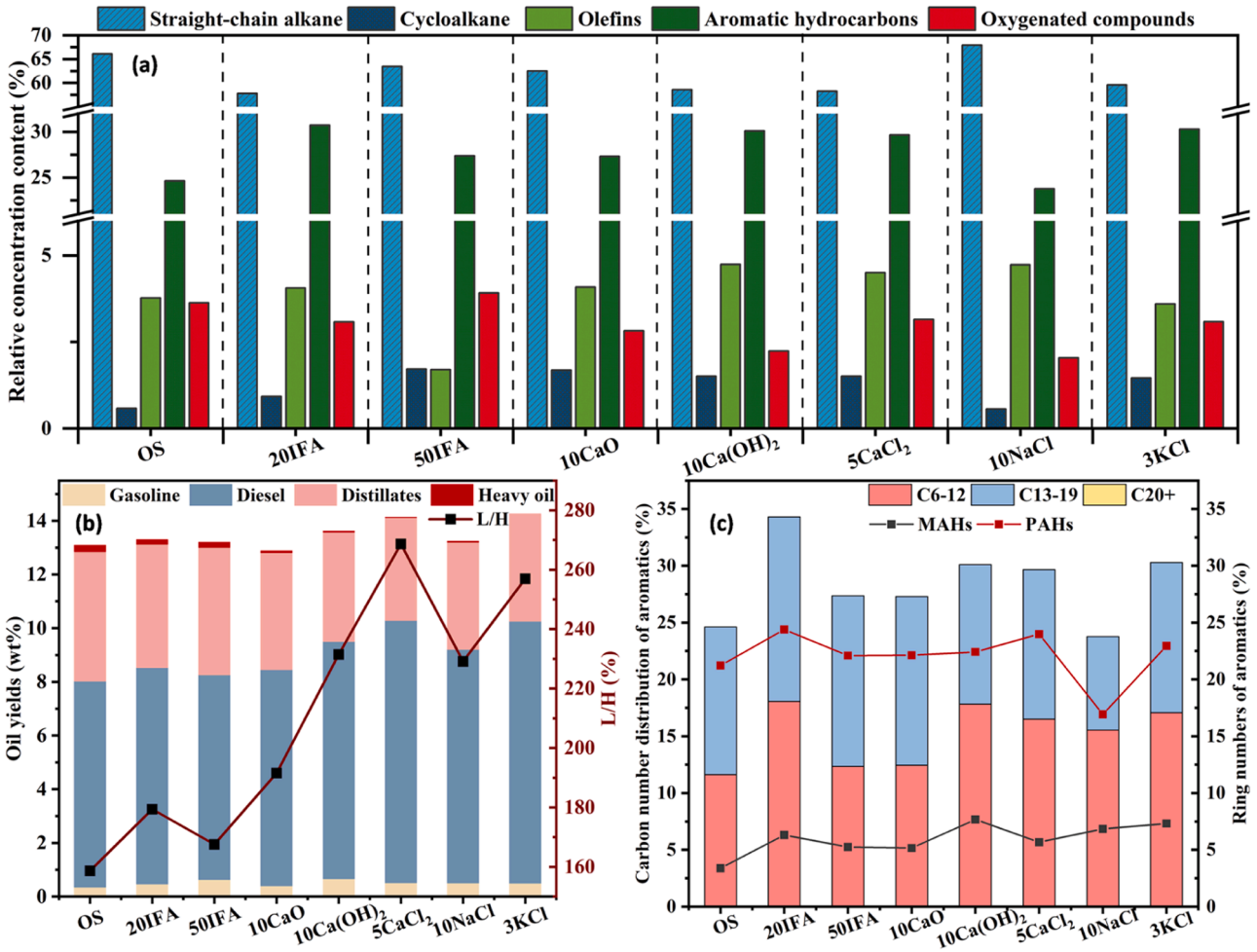

Fig. 4. Effect of IFA components addition on oil products from OS pyrolysis. (a) relative concentration content of each pyrolysis oil composition from GC-MS analysis, (b) the yields (wt%) of gasoline, diesel, distillates, and heavy oils, and (c) carbon distribution and ring numbers of aromatic hydrocarbons.

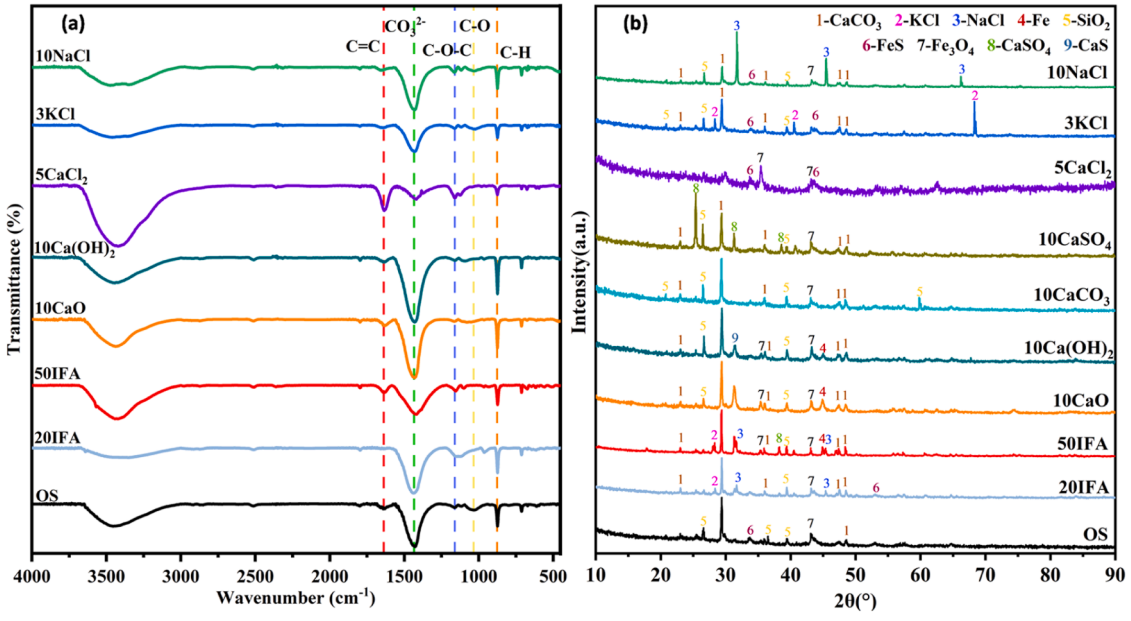

Fig. 5. (a) FTIR spectrum, and (b) XRD spectra of pyrolysis chars with different inorganic compounds addition.

[44]. To specify the variations of aromatics and straight-chain alkanes, they are categorized into different carbon number ranges, as presented in Fig. 5(c) and S7. Compared to straight-chain alkanes, the changes in aromatic hydrocarbons within the C6–12 and C13–19 ranges align closely with the light oil yield (Fig. 4a), indicating the formation of light aromatics primarily contributes to the production of lighter oil, rather than straight-chain alkanes. Moreover, the increase in monocyclic aromatic hydrocarbons (MAHs) is more significant than polycyclic aromatic hydrocarbons (PAHs). Among them, 10Ca(OH)$_2$ and 3KCl presented the highest MAHs selectivity, which increased from 3.39 % to 7.68 % and 7.33 %, respectively. The decreased proportions of straight-chain alkanes within C13–35 and increased cycloalkane and olefins content (Fig. 4b) in 5CaCl$_2$, 10Ca(OH)$_2$, 3KCl, and 10CaO demonstrate that their catalytic effect was manifested through promotion on the oligomerization, cyclization, and dehydrogenation reactions of medium to long-chain alkanes [47]. In contrast, the addition of 10 wt% NaCl had a contradictory catalytic effect. It increased the proportion of straight-chain alkanes by 1.84 % while decreasing the proportion of aromatics by 0.85 %. This effect may be attributed to its inhibition in cyclization and aromatization, as evidenced by a decrease in cycloalkanes content. However, it still improved the oil quality with an increased L/H ratio of 229.14 %, manifested by reduced PAHs content and increased MAHs content. Considering the decreased coke yield shown in Fig. 2(b), 10NaCl might have inhibited the condensation of large molecular PAHs and promoted their cracking into light aromatics, and the same phenomenon can be observed in 5CaCl$_2$, 3KCl, and 10Ca(OH)$_2$. The decreased proportion of oxygen-containing compounds in 10Ca(OH)$_2$ and 10CaO demonstrated their decarboxylation capacity due to their strong basic nature comparing to CaCl$_2$ [32,48]. The significant decrease of oxides in 10NaCl aligns with the high CO_2 production as shown in Fig. 3(a).

Comparing the individual catalytic effect of each inorganic compound to the comprehensive catalytic effect of IFA, a similar catalytic effect was observed in pyrolysis oil of 20IFA, and the amplification of aromatization may be contributed by the potential synergism between different components in IFA. However, when the addition ratio of IFA increased to 50 wt%, the catalysis effect was suppressed, which may be attributed to the competition and interference of different catalysis components and the detrimental effects conducted by $CaCO_3$ and $CaSO_4$. Furthermore, the synergistic effects of multiple components in IFA resulted in a less significant catalytic effect on improving light oil production.

3.2.4. Pyrolysis char characterization

To further study the impact of these additives addition on the pyrolysis char, FTIR was applied to investigate the functional groups, as depicted in Fig. 5(a). The drop in aromatic C═C (1640 cm^{-1}) [49,50] and C-H (874 cm^{-1}) [50] bending vibrations attributed to the addition of 10NaCl and 3KCl is consistent with decreased coke yield, as exhibited in Fig. 2(b). The disappearance of the peak at 1034 cm^{-1}, representing C-O [51], in the presence of Ca-bearing inorganic compounds suggests the potential interaction of Ca with oxygen-containing group to form C-O-Ca or COO-Ca [20,52] according to the neutralization reaction as shown in Eq. (10) [12,32]. This interaction activated the oxygen sites and increased the likelihood of cracking into lighter compounds [53]. However, the significant increase in C-O-C bending vibration and aromatic C═C bond intensity with the addition of 5 wt% CaCl$_2$ suggest its capacity of immobilizing oxygenated organic matter during the pyrolysis [54], explaining the considerable low CO_2 release as shown in Fig. 3(a) and the lower calcite bond intensity. The enhanced calcite bonds at 1428 cm^{-1} [55] confirmed that the emitted CO_2 was adsorbed by CaO and 10Ca(OH)$_2$ and retained as $CaCO_3$ in the co-pyrolysis char. Therefore, both CaO, Ca(OH)$_2$, and alkali chlorides contribute to the deoxygenation reactions during IFA catalyzed OS pyrolysis.

$$R-COOH+R'-COOH+CaO \leftrightarrow R-COO-Ca-OOC-R'+H_2O \quad (10)$$

3.3. Effect of IFA addition on inherent Fe species in OS during co-pyrolysis

According to our previous research [20], iron-based substances in OS went through a reduction reaction during the co-pyrolysis of OS with IFA, and their phase transformations are further investigated in this study through XRD, XPS, and SEM-EDS.

As exhibited in Fig. 5(b), the major minerals detected in the OS pyrolysis char are $CaCO_3$, SiO_2, and FeS. Interestingly, apart from 20IFA and 50IFA [20], an additional diffraction peak is evident at about 2θ= 44.90° in 10CaO, 10Ca(OH)$_2$, which is attributed to the diffraction of Fe (110) [56]. However, only FeS and Fe_3O_4 were detected in chars with other additives. This finding suggests that, in comparison to chlorides, CaO and Ca(OH)$_2$ may play a crucial role in inducing the reduction of Fe species during pyrolysis, possibly due to the significant increased H_2 formation, as shown in Fig. 3(a). XPS results of Fe 2p in chars further support the observed chemical state transformation of Fe during co-pyrolysis, and the peaks were fitted with the software of Avantage (Fig. 6). The binding energy for Fe (III) is larger than Fe (II) [57,58], and the peak area ratios were utilized for the semi-quantification of the concentrations [53]. Here, concentration ratios of Fe in different valence states are presented in Table S1, and a high iron reduction degree was presented with 50 wt% IFA addition. Moreover, the additions of calcium-bearing substances and chlorides all promoted the reduction of inherent iron-based substances in OS during catalytic pyrolysis [59]. However, as the XPS only focuses on a narrow and thin layer[53], it detects the meagre presence of metallic Fe in the samples [60].

The microstructural analysis of pyrolysis chars with IFA and IFA components addition is depicted in Fig. 7 and Fig. S8, respectively. The pyrolysis char particles from OS (Fig. 7a) displayed a dense structure, which transitioned to a clustered and porous configuration with the addition of additives. The porous morphology observed in 50IFA (Fig. 7c), 5CaCl$_2$ (Fig. S8c), and 3KCl (Fig. S8d) is attributed to increased surface cavities resulting from enhanced reactions and the release of gaseous products. The quantified EDS results revealed that additives reduced the carbon deposition on particle surfaces. Furthermore, in the 20IFA (Fig. 7b) and 50IFA chars, there was a notably higher Fe content compared to Ca content when compared to OS char. This trend was consistent across chars with various IFA component additions, particularly evident in 10CaO (Fig. S8a) and 10Ca(OH)$_2$ (Fig. S8b).

In conclusion, IFA components decreased surface coke coverage and facilitated the dispersion of inherent Fe species, leading to a greater proportion of iron-based species engaged in the catalytic pyrolysis of oily sludge as an inherent catalyst. Based on previous reports, the release of lattice oxygen in Fe_2O_3 could assist the depolymerization of polycyclic substances and convert it into MAHs with reduced coke formation [61,62]. Research on catalytic coal pyrolysis conducted by He et al. suggests that AAEM can activate carbon sites by interacting with oxygen-containing functional groups and forming active Fe-(O)-C on the char surface [53], assisting in the decomposition of heavy compounds. However, quantifying the contributions of inherent Fe species and IFA components to catalytic pyrolysis is challenging due to the complexity of the OS solid fraction. Moreover, the proportion of Fe reduction caused by engagement in catalytic pyrolysis and reduction by H_2 should be distinguished in future work.

3.4. Catalytic mechanism of IFA on OS pyrolysis

During the co-pyrolysis of OS and IFA, each IFA component played distinct catalytic roles in modifying product distributions and product properties, as depicted in Fig. 8. In the pyrolysis gas, all the inorganic

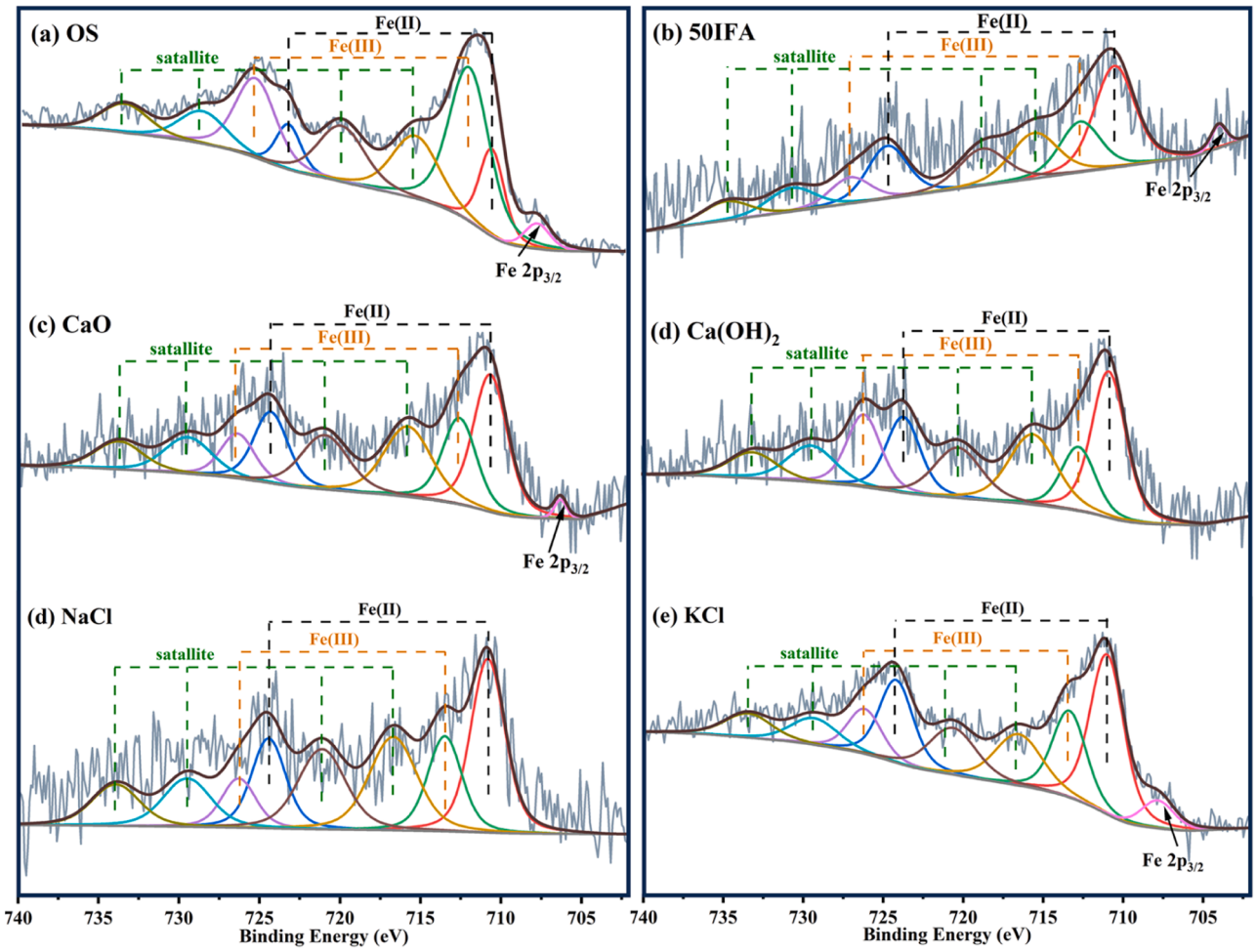

Fig. 6. XPS spectra of Fe 2p for the chars obtained from pyrolysis samples of (a) OS, (b) 50IFA, (c) 10CaO, (D) 10$Ca(OH)_2$, (e) 10NaCl, and (f) 3KCl.

compounds in IFA, particularly KCl and NaCl, promoted the decomposition of oxygen-containing compounds in OS, with increased CO and CO_2 production. However, the generated CO_2 was fully absorbed by Ca$(OH)_2$ and CaO, while CO was consumed via the water-gas shift reaction to produce H_2, primarily facilitated by $Ca(OH)_2$ and inherent Fe species. Additionally, these components promoted dehydrogenation reactions, resulting in a substantial increase in H_2 selectivity in pyrolysis gas. The combined effect of each component in IFA further amplified, leading to a synergistic enhancement in H_2 production. On the other hand, the cleavage of aliphatic side chains was promoted by KCl and NaCl, which contributes to higher C1-C3 hydrocarbons production in 20IFA and 50IFA.

Regarding the pyrolysis oil, $Ca(OH)_2$, $CaCl_2$, and KCl intensified the cracking of middle and long-chain alkanes, resulting in a greater ratio of short-chain alkanes and increased aromatics formation. During the co-pyrolysis, the formation of light aromatics, particularly MAHs, led to increased light oil yield. This aromatization process was enhanced through two pathways, as illustrated in Fig. 8. Enhanced Diels–Alder reactions promoted the production of MAHs [63], as evidenced by the higher olefin proportion in the pyrolysis oil and the strengthened dehydrogenation reactions [64]. Furthermore, existing GC-MS data shown in Fig. 4 supports the notion that the presence of $Ca(OH)_2$, CaO, KCl, and $CaCl_2$ facilitates the production of light aromatics through dehydrogenation, cyclization, and further dehydrogenation reactions [65], as illustrated in the second path. In contrast, NaCl presented a different catalysis effect, which retarded the aromatization of alkanes through limiting the formation of cycloalkanes. However, it effectively promoted the decomposition of PAHs into light aromatics. Similar effects were observed in 10$Ca(OH)_2$, 3KCl, and 5$CaCl_2$.

In the pyrolysis char, the addition of chlorides and $Ca(OH)_2$ effectively inhibited the condensation of heavy organic compounds and the un-desired re-condensations of the light aromatics [63], which significantly reduced coke formation. However, the presence of $CaCO_3$ and $CaSO_4$ promoted condensation reactions and increased coke formation.

The varying proportions of different IFA components resulted in different contributions to the overall catalytic effects on the co-pyrolysis process. $Ca(OH)_2$, as the predominant inorganic compounds in IFA, played a crucial role in enhancing H_2 selectivity and promoting the formation of light aromatics, and its catalytic effect was further enhanced with increased addition concentrations. In contrast, even at low concentrations, KCl exhibited an important effect on promoting the formation of C1-C3 hydrocarbons and improving the quality of pyrolysis oil. Furthermore, our study revealed that IFA compounds facilitated the uniform distribution of the intrinsic iron-based species of OS on the pyrolysis char surface, which promoted their active participation in the in-situ catalytic pyrolysis of OS. Additionally, the presence of metallic Fe in the chars with $Ca(OH)_2$ and CaO addition suggested that the increased presence of H_2 may facilitate their subsequent reduction. However, the synergistic effect of multiple components may inhibit the conversion of coke from solid to volatiles, albeit to a limited extent, and the overall catalytic effect of IFA on enhancing the recovery rate of pyrolysis oil is not as pronounced as that of individual active chemicals.

Apart from oily sludge, IFA holds promise as a catalyst for pyrolyzing other organic-rich waste materials, leveraging its catalytic effects and mechanisms. Additionally, our study underscores the selective role of alkali salts and calcium-containing minerals in shaping pyrolysis

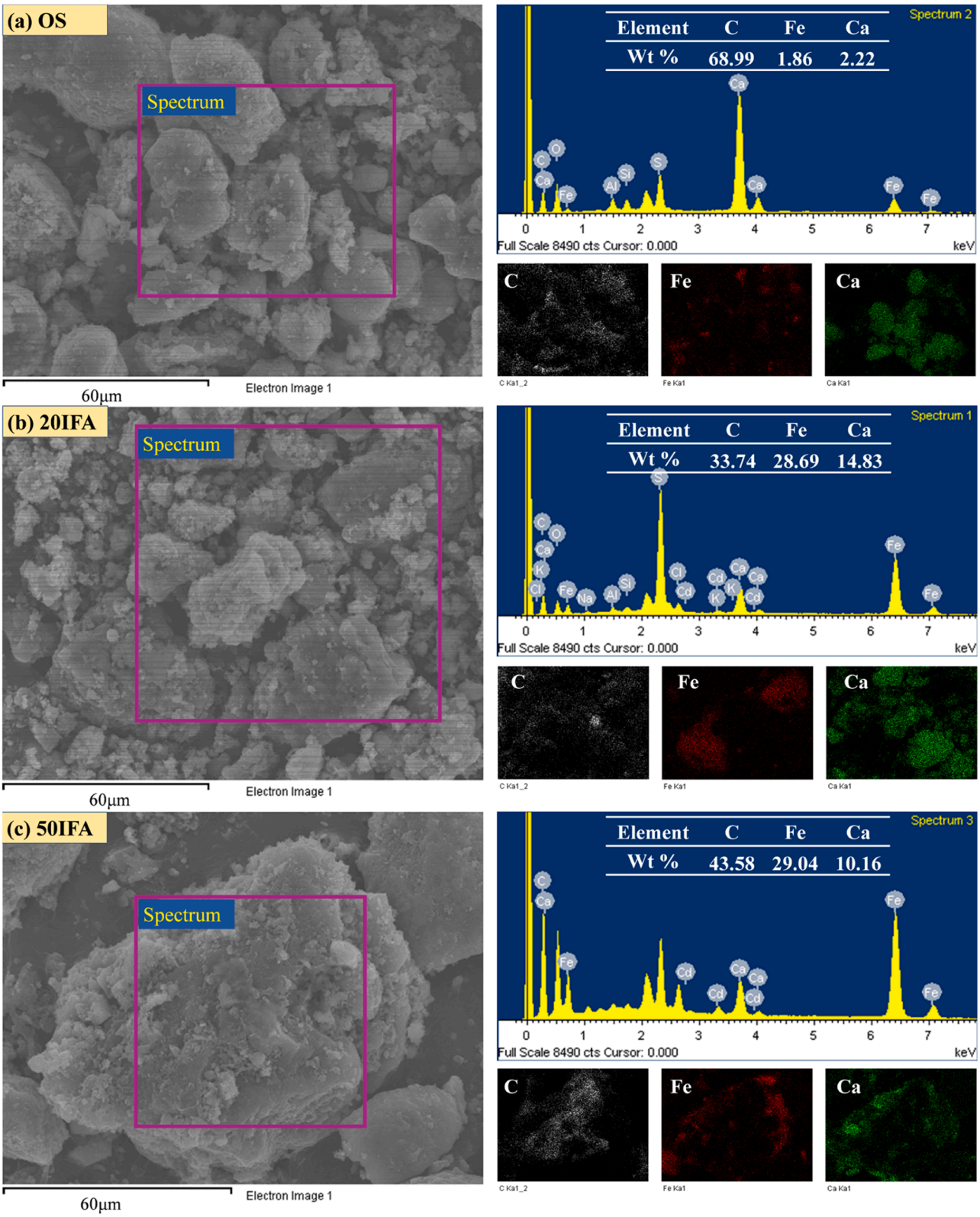

Fig. 7. SEM and EDS analyses of pyrolysis chars: (a) OS, (b) 20IFA, and (c) 50IFA.

product formation, thereby broadening the potential for utilizing wastes containing these components.

4. Conclusion

This study delves into the catalytic impacts of various inorganic compounds in IFA on the distribution and properties of OS pyrolysis products at 600 °C, as well as their distinct contributions to the overall catalytic activity of IFA during the co-pyrolysis. The cumulative catalytic effects lead to improved pyrolysis gas quality and decreased coke formation. However, it is worth noting that these component interactions do not exhibit a straightforward cumulative impact on the

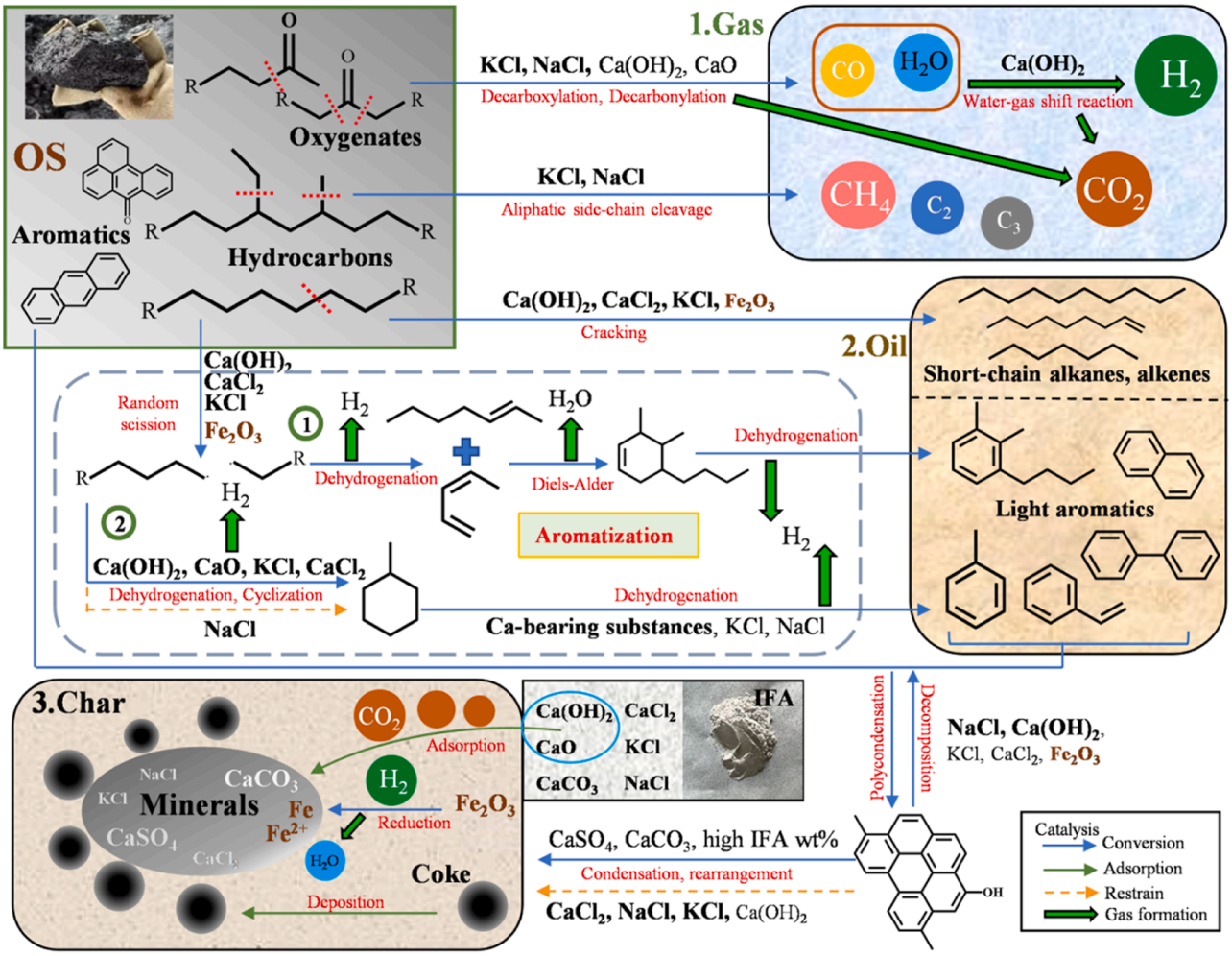

Fig. 8. Proposed mechanism of co-pyrolysis of IFA and OS with the functions of each IFA compound.

resulting pyrolysis oil at high addition ratios.

The specific conclusions are as follows: (1) The synergistic effect of multiple components in IFA on enhancing oil yield and suppressing coke formation is less pronounced compared to its individual components. (2) CaO, $Ca(OH)_2$, and chlorides could inhibit the condensation of PAHs and coke formation, while $CaSO_4$ and $CaCO_3$ exhibit contradictory results. (3) $Ca(OH)_2$ contributes the most to increasing H_2 selectivity through enhancing dehydrogenation and water-gas shift reaction, and higher $Ca(OH)_2$ content further strengthens this effect. (4) CaO, $Ca(OH)_2$, and alkali metal chlorides in IFA promote deoxygenation reaction, while $CaCl_2$ stabilizes oxygenated compounds. Additionally, the CO_2 adsorption capacity of CaO and $Ca(OH)_2$ contributes to CO_2 mitigation. (5) $Ca(OH)_2$, $CaCl_2$, and KCl effectively promote the cracking of long and middle-chain alkanes and facilitate light aromatic formation, while NaCl has the opposite effect. (6) IFA components aid in dispersing inherent iron-based species of OS on the char surface, facilitating their involvement in in-situ OS catalytic pyrolysis, and the produced H_2 during co-pyrolysis accelerates its reduction.

Overall, this study improves our understanding of the catalytic mechanism of IFA during the co-pyrolysis with OS. Each inorganic compound in IFA exhibits different selectivity in catalyzing pyrolysis reactions, offering valuable insights for enhancing pyrolysis products specificity and selectivity. This discovery expands the potential of solid waste as a catalyst and provides valuable insights into co-processing solid waste to create value-added products.

CRediT authorship contribution statement

Yin Wang: Writing – review & editing, Supervision, Resources, Project administration, Funding acquisition, Conceptualization. **Jun He:** Writing – review & editing, Supervision. **Hao Yu:** Data curation. **Bo Li:** Writing – review & editing. **Jie Li:** Writing – review & editing, Conceptualization. **Zhiwei Li:** Writing – review & editing. **Di Yu:** Writing – review & editing, Writing – original draft, Validation, Software, Methodology, Investigation, Formal analysis, Data curation.

Declaration of Competing Interest

The authors declare that they have no known competing financial interests or personal relationships that could have appeared to influence the work reported in this paper.

Data availability

Data will be made available on request.

Acknowledgements

This work was jointly supported by the Major Special Project of Fujian Province [Grant No. 2023YZ038009], Ningbo S&T Project (2021-DST-004), the Alliance of International Science Organizations [Grant No. ANSO-CR-KP-2021-08], STS Plan Supporting Project of the Chinese Academy of Sciences in Fujian Province [Grant Nos. 2020T3036,

2021T3102, 2021T3073, 2021T3049, 2022T3065], the Social Development Leading Key Projects of Fujian Province [Grant No. 2023Y0074, 2022Y0080, 2021Y0069], Ningbo Bureau of Science and Technology (2022Z028, 2023J024, 2023S038), and Zhejiang Key R&D Programme (No. 2023C03146) funded by the Zhejiang Provincial Department of Science and Technology.

Appendix A. Supporting information

Supplementary data associated with this article can be found in the online version at doi:10.1016/j.jhazmat.2024.134368.

References

[1] Wang, G., Wang, L., Li, L., Chen, Y., Cao, W., Jin, H., et al., 2023. Oil diffusion mathematical model in oily sludge particle under supercritical water environment. J Hazard Mater 443, 130348.
[2] Dal Mas, F., Zeng, X., Huang, Q., Li, J., 2021. Quantifying material flow of oily sludge in China and its implications. J Environ Manag 287, 112115.
[3] Li, J., Lin, F., Li, K., Zheng, F., Yan, B., Che, L., et al., 2021. A critical review on energy recovery and non-hazardous disposal of oily sludge from petroleum industry by pyrolysis. J Hazard Mater 406, 124706.
[4] Chen, Z., Zheng, Z., He, C., Liu, J., Zhang, R., Chen, Q., 2022. Oily sludge treatment in subcritical and supercritical water: A review. J Hazard Mater, 128761.
[5] Chen, L., Zhang, X., Sun, L., Xu, H., Si, H., Mei, N., 2016. Study on the fast pyrolysis of oil sludge and its product distribution by PY-GC/MS. Energy Fuels 30 (12), 10222–10227.
[6] Li, J., Lin, F., Xiang, L., Zheng, F., Che, L., Tian, W., et al., 2021. Hazardous elements flow during pyrolysis of oily sludge. J Hazard Mater 409, 124986.
[7] Lin, B., Huang, Q., Ali, M., Wang, F., Chi, Y., Yan, J., 2019. Continuous catalytic pyrolysis of oily sludge using U-shape reactor for producing saturates-enriched light oil. Proc Combust Inst 37 (3), 3101–3108.
[8] Quan, C., Zhang, G., Xu, L., Wang, J., Gao, N., 2022. Improvement of the pyrolysis products of oily sludge: catalysts and catalytic process. J Energy Inst.
[9] Milato, J.V., Franca, R.J., Calderari, M.R.M., 2020. Co-pyrolysis of oil sludge with polyolefins: evaluation of different Y zeolites to obtain paraffinic products. J Environ Chem Eng 8 (3), 103805.
[10] Lin, B., Wang, J., Huang, Q., Ali, M., Chi, Y., 2017. Aromatic recovery from distillate oil of oily sludge through catalytic pyrolysis over Zn modified HZSM-5 zeolites. J Anal Appl Pyrolysis 128, 291–303.
[11] Shie, J.-L., Lin, J.-P., Chang, C.-Y., Lee, D.-J., Wu, C.-H., 2003. Pyrolysis of oil sludge with additives of sodium and potassium compounds. Resour, Conserv Recycl 39 (1), 51–64.
[12] Zhang, W., He, Y., Xing, X., Wang, Y., Li, Q., Wang, L., et al., 2023. In-depth insight into the effects of intrinsic calcium compounds on the pyrolysis of hazardous petrochemical sludge. J Hazard Mater 455, 131593.
[13] Gao, N., Li, J., Quan, C., Tan, H., 2020. Product property and environmental risk assessment of heavy metals during pyrolysis of oily sludge with fly ash additive. Fuel 266, 117090.
[14] Lin, F., Zheng, F., Li, J., Sun, B., Che, L., Yan, B., et al., 2022. Catalytic pyrolysis of oily sludge with iron-containing waste for production of high-quality oil and H2-rich gas. Fuel 326, 124995.
[15] Wang, L., Zhang, Y., Chen, L., Guo, B., Tan, Y., Sasaki, K., et al., 2022. Designing novel magnesium oxysulfate cement for stabilization/solidification of municipal solid waste incineration fly ash. J Hazard Mater 423, 127025.
[16] Zhang, Y., Wang, L., Chen, L., Ma, B., Zhang, Y., Ni, W., et al., 2021. Treatment of municipal solid waste incineration fly ash: State-of-the-art technologies and future perspectives. J Hazard Mater 411, 125132.
[17] Assi, A., Bilo, F., Zanoletti, A., Ponti, J., Valsesia, A., La Spina, R., et al., 2020. Zero-waste approach in municipal solid waste incineration: Reuse of bottom ash to stabilize fly ash. J Clean Prod 245, 118779.
[18] Ren, J., Liu, B., Guo, J., Liu, J., Xing, F., Zhu, H., et al., 2024. Bio-treatment of municipal solid waste incineration fly ash: A sustainable path for recyclability. J Clean Prod 434, 139869.
[19] Fujii, T., Kashimura, K., Tanaka, H., 2019. Microwave sintering of fly ash containing unburnt carbon and sodium chloride. J Hazard Mater 369, 318–323.
[20] Yu, D., Li, Z., Li, J., He, J., Li, B., Wang, Y., 2023. Enhancement of H2 and light oil production and CO_2 emission mitigation during co-pyrolysis of oily sludge and incineration fly ash. J Hazard Mater, 132618.
[21] Giudicianni, P., Gargiulo, V., Grottola, C.M., Alfè, M., Ferreiro, A.I., Mendes, M.A. A., Fagnano, M., Ragucci, R., 2021. Inherent metal elements in biomass pyrolysis: a review. Energy Fuels 35 (7), 5407–5478.
[22] Heng, J., Tan, T., Xing, Z., Ong, J., Lin, K., Koh, X., et al., 2023. Unraveling the catalytic activity of CaClOH-rich incineration fly ash in the pyrolysis of single-use plastics. Mater Today Chem 31, 101608.
[23] Gong, Z., Liu, C., Wang, M., Wang, Z., Li, X., 2020. Experimental study on catalytic pyrolysis of oil sludge under mild temperature. Sci Total Environ 708, 135039.
[24] International, A., 2018. Standard Test Method for Water in Petroleum Products and Bituminous Materials by Distillation. ASTM D95–13.
[25] Liu, Z., Fang, W., Cai, Z., Zhang, J., Yue, Y., Qian, G., 2022. Garbage-classification policy changes characteristics of municipal-solid-waste fly ash in China. Sci Total Environ, 159299.
[26] Wang, H., Zhao, B., Zhu, F., Chen, Q., Zhou, T., Wang, Y., 2023. Study on the reduction of chlorine and heavy metals in municipal solid waste incineration fly ash by organic acid and microwave treatment and the variation of environmental risk of heavy metals. Sci Total Environ, 161929.
[27] Wang, Y., Zhang, Y., Xu, J., Zhong, J., Wei, F., Zhang, J., et al., 2022. Footprints in compositions, PCDD/Fs and heavy metals in medical waste fly ash: large-scale evidence from 17 medical waste thermochemical disposal facilities across China. J Hazard Mater, 130471.
[28] Gong, Z., Du, A., Wang, Z., Fang, P., Li, X., 2017. Experimental study on pyrolysis characteristics of oil sludge with a tube furnace reactor. Energy Fuels 31 (8), 8102–8108.
[29] Day, S.J., Killingley, J.S., 1993. Coke formation on recycled combusted Rundle oil shale. Fuel 72 (1), 119–124.
[30] Lai, D., Shi, Y., Geng, S., Chen, Z., Gao, S., Zhan, J.-H., et al., 2016. Secondary reactions in oil shale pyrolysis by solid heat carrier in a moving bed with internals. Fuel 173, 138–145.
[31] Li, J., Zheng, F., Li, Q., Farooq, M.Z., Lin, F., Yuan, D., et al., 2022. Effects of inherent minerals on oily sludge pyrolysis: Kinetics, products, and secondary pollutants. Chem Eng J 431, 133218.
[32] Zhang, Y., Cui, H., Yi, W., Song, F., Zhao, P., Wang, L., et al., 2017. Highly effective decarboxylation of the carboxylic acids in fast pyrolysis oil of rice husk towards ketones using CaCO3 as a recyclable agent. Biomass– Bioenergy 102, 13–22.
[33] Li, K., Li, Y., Jiang, Y., Zou, Y., Wu, X., Yang, Y., 2023. A study on self-shielding effect of CaCO3 in cable pyrolysis using gas product analysis and PSO optimization. Fire Saf J 140, 103917.
[34] Li, L., Wang, G., Li, X., Wang, L., Zhang, J., Cheng, K., et al., 2023. Experimental study on alkali catalytic gasification of oily sludge in supercritical water with a continuous reactor. J Environ Manag 327, 116957.
[35] Wang, D., Wang, D., Yu, J., Chen, Z., Li, Y., Gao, S., 2019. Role of alkali sodium on the catalytic performance of red mud during coal pyrolysis. Fuel Process Technol 186, 81–87.
[36] Yao, D., Wu, C., Yang, H., Zhang, Y., Nahil, M.A., Chen, Y., et al., 2017. Co-production of hydrogen and carbon nanotubes from catalytic pyrolysis of waste plastics on Ni-Fe bimetallic catalyst. Energy Convers Manag 148, 692–700.
[37] Veses, A., Aznar, M., López, J., Callén, M., Murillo, R., García, T., 2015. Production of upgraded bio-oils by biomass catalytic pyrolysis in an auger reactor using low cost materials. Fuel 141, 17–22.
[38] Wu, B., Guo, X., Qian, X., Liu, B., 2022. Insight into the influence of calcium on the co-pyrolysis of coal and polystyrene. Fuel 329, 125471.
[39] Zeng, X., Wang, Y., Yu, J., Wu, S., Zhong, M., Xu, S., et al., 2011. Coal pyrolysis in a fluidized bed for adapting to a two-stage gasification process. Energy fuels 25 (3), 1092–1098.
[40] Alcazar-Ruiz, A., Ortiz, M.L., Sanchez-Silva, L., Dorado, F., 2021. Catalytic effect of alkali and alkaline earth metals on fast pyrolysis pre-treatment of agricultural waste. Biofuels, Bioprod Bioref 15 (5), 1473–1484.
[41] Wang, Y., Li, Y., Wang, G., Zhu, J., Yang, H., Jin, L., et al., 2022. In-situ catalytic upgrading of coal pyrolysis volatiles over red mud-supported nickel catalysts. Fuel 324, 124742.
[42] Jiang, L., Liu, C., Hu, S., Wang, Y., Xu, K., Su, S., et al., 2018. Catalytic behaviors of alkali metal salt involved in homogeneous volatile and heterogeneous char reforming in steam gasification of cellulose. Energy Convers Manag 158, 147–155.
[43] Zhang, Y., Wang, J., Lv, P., Bie, N., Cao, P., Bai, Y., et al., 2022. Capture of released alkali metals and its simultaneously catalytic performance on secondary reactions of volatiles during biomass pyrolysis. Fuel 317, 123557.
[44] Lin, F., Yu, H., Li, J., Zygourakis, K., Li, R., Cheng, Z., et al., 2023. Investigation on the interaction between oil compositions and soil minerals with the targets of resource recovery and harmless disposal of oily sludges by pyrolysis. ACS EST Eng 3 (5), 734–744.
[45] Wang, Y., Li, Y., Wang, G., Wu, Y., Yang, H., Jin, L., et al., 2022. Effect of Fe components in red mud on catalytic pyrolysis of low rank coal. J Energy Inst 100, 1–9.
[46] Kang, S., Zhang, S., Wang, Z., Li, S., Zhao, F., Yang, J., et al., 2023. Highly efficient catalytic pyrolysis of oil shale by CaCl2 in subcritical water. Energy 274, 127343.
[47] Wang, W., Yao, C., Ge, X., Pu, X., Yuan, J., Sun, W., et al., 2023. Catalytic Conversion of Polyethylene into Aromatics with Pt/ZSM-5: Insights on Reaction Pathways and Rate-Controlling Step Regulation. J Mater Chem A.
[48] Kumagai, S., Yamasaki, R., Kameda, T., Saito, Y., Watanabe, A., Watanabe, C., et al., 2018. Aromatic hydrocarbon selectivity as a function of CaO basicity and aging during CaO-catalyzed PET pyrolysis using tandem μ-reactor-GC/MS. Chem Eng J 332, 169–173.
[49] Ban, Y., Jin, L., Zhu, J., Liu, F., Hu, H., 2022. Insights into effect of Ca (OH) 2 on pyrolysis behaviors and products distribution of Hongshaquan coal. Fuel 307, 121791.
[50] Keiluweit, M., Nico, P.S., Johnson, M.G., Kleber, M., 2010. Dynamic molecular structure of plant biomass-derived black carbon (biochar). Environ Sci Technol 44 (4), 1247–1253.
[51] Mo, W., Wu, Z., He, X., Qiang, W., Wei, B., Wei, X., et al., 2021. Functional group characteristics and pyrolysis/combustion performance of fly ashes from Karamay oily sludge based on FT-IR and TG-DTG analyses. Fuel 296, 120669.
[52] Zou, X., Yao, J., Yang, X., Song, W., Lin, W., 2007. Catalytic effects of metal chlorides on the pyrolysis of lignite. Energy Fuels 21 (2), 619–624.
[53] He, R., Deng, J., Deng, X., Xie, X., Li, Y., Yuan, S., 2022. Effects of alkali and alkaline earth metals of inherent minerals on Fe-catalyzed coal pyrolysis. Energy 238, 121985.

[54] Shao, F., Xu, J., Kang, X., Hu, Z., Shao, Y., Lu, C., et al., 2023. An attempt to enhance the adsorption capacity of biochar for organic pollutants-Characteristics of CaCl2 biochar under multiple design conditions. Sci Total Environ 854, 158675.
[55] Reig, F.B., Adelantado, J.G., Moreno, M.M., 2002. FTIR quantitative analysis of calcium carbonate (calcite) and silica (quartz) mixtures using the constant ratio method. Application to geological samples. Talanta 58 (4), 811–821.
[56] Wu, X., Zhang, Z., Liang, Q., Meng, J., 2012. Evolution from (110) Fe to (111) Fe3O4 thin films grown by magnetron sputtering using Fe2O3 target. J Cryst Growth 340 (1), 74–77.
[57] Song, Q., Zhao, H., Chang, S., Yang, L., Zou, F., Shu, X., et al., 2020. Study on the catalytic pyrolysis of coal volatiles over hematite for the production of light tar. J Anal Appl Pyrolysis 151, 104927.
[58] Yamashita, T., Hayes, P., 2008. Analysis of XPS spectra of Fe2+ and Fe3+ ions in oxide materials. Appl Surf Sci 254 (8), 2441–2449.
[59] Li, P., Zhang, X., Wang, J., Guo, H., Chen, Y., Wang, Z., et al., 2020. Process characteristics of catalytic thermochemical conversion of oily sludge with addition of steel slag towards energy and iron recovery. J Environ Chem Eng 8 (4), 103911.
[60] Suzuki, S., Yanagihara, K., Hirokawa, K., 2000. XPS study of oxides formed on the surface of high-purity iron exposed to air. Surf Interface Anal: Int J Devoted Dev Appl Tech Anal Surf, Interfaces thin films 30 (1), 372–376.
[61] Shi, P., Chang, G., Tan, X., Guo, Q., 2020. Enhancement of bituminous coal pyrolysis for BTX production by Fe2O3/MoSi2-HZSM-5 catalysts. J Anal Appl Pyrolysis 150, 104867.
[62] Sun, K., Themelis, N.J., Bourtsalas, A.T., Huang, Q., 2020. Selective production of aromatics from waste plastic pyrolysis by using sewage sludge derived char catalyst. J Clean Prod 268, 122038.
[63] He, Y., Chen, J., Mo, Z., Hu, C., Li, D., Tu, J., et al., 2023. Controlling Diels-Alder reactions in catalytic pyrolysis of sawdust and polypropylene by coupling CO_2 atmosphere and Fe-modified zeolite for enhanced light aromatics production. J Hazard Mater 455, 131547.
[64] Ma, Z., Sun, Q., Ye, J., Yao, Q., Zhao, C., 2016. Study on the thermal degradation behaviors and kinetics of alkali lignin for production of phenolic-rich bio-oil using TGA–FTIR and Py–GC/MS. J Anal Appl Pyrolysis 117, 116–124.
[65] Liu, P., Wang, J., Ling, L., Shen, X., Li, X., Zhang, R., et al., 2024. Suitable location of Lewis acid over ZnOH+/HZSM-5 catalysts effectively enhance dehydrogenation activity and catalyze the aromatization process of C6 olefins in MTA. Fuel 357, 130000.